

Concept of an Automotive LiDAR Target Simulator for Direct Time-of-Flight LiDAR

Sara Grollius , Manuel Ligges , Jennifer Ruskowski, and Anton Grabmaier 

Abstract—Autonomous driving can make traffic safer by reducing human errors. Different sensor types in autonomous vehicles could introduce additional technical failures. We offer a target simulator testing LiDAR systems under automotive conditions. Therefore, data are projected over-the-air by laser signals on the LiDAR detector. This work presents a concept of a LiDAR target simulator with regards to LiDAR systems using the direct time-of-flight principle. We develop design considerations for a screen discussing undesired screen reflections, a curved screen form and the positioning of light sources on this screen. As one main solution, we introduce a concept of an antireflective screen. For the scenario simulation, we derive a model delivering the required optical power representing a simulated target, which is combined with the simulated time-of-flight. Considering no prior knowledge of the LiDAR system under test, we discuss the required calibration data and timing resolution. Thereby, we suggest an optimized time-of-flight concept requiring only one optical trigger to determine the LiDAR measurement start. All requirements are supported by calculated example parameters based on real LiDAR systems. Altogether, we discuss main challenges and possible solutions of our LiDAR target simulator, which will allow a safer and more efficient development of LiDAR systems.

Index Terms—Time-of-flight (ToF), light detection and ranging (LiDAR) testing, LiDAR target simulator, device-under-test (DUT), LiDAR-under-test (LUT), hardware-in-the-loop (HiL), over-the-air (OTA).

I. INTRODUCTION

ALTHOUGH one feels very safe about driving, a frequent reason for death is human error in traffic. Therefore, advanced driver-assistance systems (ADAS) are developed to compensate human inattentiveness. With autonomous driving, new possibilities of driving failures arise. Even though there might be less technical errors than human error sources, the validation of autonomous sensors is very important. Sensor testing supports the trust in autonomous driving, which is needed to introduce new technological developments in our society. To

Manuscript received 14 April 2021; revised 8 September 2021; accepted 9 November 2021. Date of publication 17 November 2021; date of current version 23 January 2023. (Corresponding author: Sara Grollius.)

Sara Grollius, Manuel Ligges, and Jennifer Ruskowski are with the Fraunhofer Institute for Microelectronic Circuits and Systems, 47057 Duisburg, Germany (e-mail: sara.grollius@ims.fraunhofer.de; manuel.ligges@ims.fraunhofer.de; jennifer.ruskowski@ims.fraunhofer.de).

Anton Grabmaier is with the Fraunhofer Institute for Microelectronic Circuits and Systems, 47057 Duisburg, Germany, and also with the University of Duisburg-Essen, 47057 Duisburg, Germany (e-mail: anton.grabmaier@ims.fraunhofer.de).

Color versions of one or more figures in this article are available at <https://doi.org/10.1109/TIV.2021.3128808>.

Digital Object Identifier 10.1109/TIV.2021.3128808

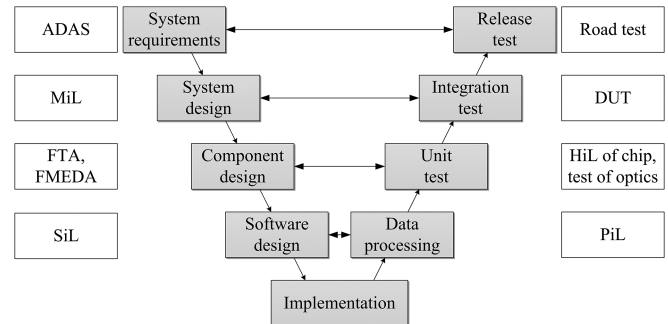


Fig. 1. Target simulator with device-under-test (DUT) as part of V-model for ADAS sensor systems.

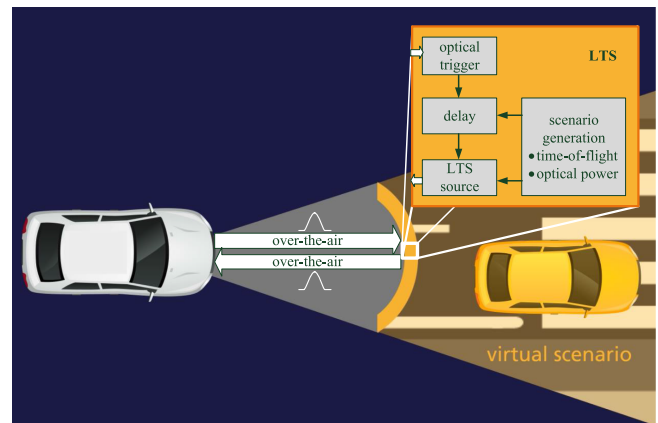


Fig. 2. Concept of LiDAR target simulator as screen delivering data over-the-air (OTA).

keep society's acceptance and make autonomous driving as safe as it is needed, sensors must be proven in their right practicality. Many development and testing procedures exist to validate autonomous sensors like model-in-the-loop (MiL), fault tree analysis (FTA) or Failure Modes Effects and Diagnostic Analysis (FMEDA), software-in-the-loop (SiL), processor-in-the-loop (PiL), hardware-in-the-loop (HiL) for single components and road tests on testing roads or even in real traffic (Fig. 1). To complete these methods, a target simulator is considered for the device-under-test (DUT). The scenarios are produced by simulation or by real measurements. Different to a HiL with hardware connection to the sensor, these scenarios are transferred to the sensor system over-the-air (OTA) (Fig. 2).

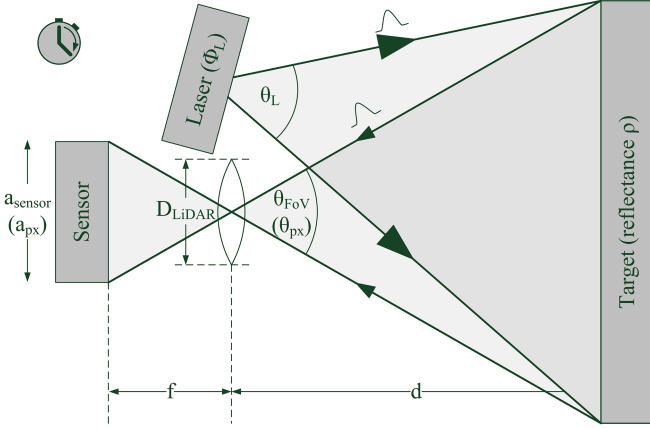


Fig. 3. Principle of light detection and ranging (LiDAR).

One promising sensor technology is the method of light detection and ranging (LiDAR). A LiDAR system emits a laser signal that is reflected by a target and then measured by the LiDAR detector (Fig. 3). In the following, LiDAR systems with the principle of direct time-of-flight (dToF) using short laser pulses are applied. Due to the known speed of light c , their measurement of the laser time-of-flight (ToF) t directly determines the distance d [1] by

$$d = \frac{c \cdot t}{2}. \quad (1)$$

The LiDAR-under-test (LUT) can be tested by a LiDAR target simulator (LTS). The LTS takes measurements or theoretically defined scenarios and projects the data on the sensor by laser signals. Therefore, this testing procedure is also called over-the-air (OTA) stimulation. In this way, the receiver module of the LiDAR system and the underlying algorithms as well as their interaction are validated. Comparing the measured data of the sensor to the original data proves the sensor's mode of operation.

The LTS can already be used at the development stage of a LiDAR detector and to validate the final LiDAR system. Besides the validation, the testing delivers a benchmarking of LiDAR sensors from different manufacturers and supports the development of standard tests. An LTS shows the potential of testing a broad spectrum of scenarios without requiring many resources. Compared to real driving tests, it can provide any traffic scenario at any time independent from the current weather conditions. Therefore, the scenarios are reproducible and can run continuously, i.e. over night as well. Collision scenes can be tested virtually without destroying the vehicle or a modeled environment. Altogether, an LTS is a cost-effective and safe testing method, which also allows for comparability and verification of different system design specifications.

For cameras and radar sensors some research on target simulators already exists [2]–[4]. Furthermore, a long-range LTS up to 2.5 km, which is often applied to military purpose, has been discussed [5], [6]. The development of an LTS is mentioned by some companies [7]. There are two patents with concepts of LiDAR target simulators [8], [9]. Currently, no completely realized LTS exists.

For automotive LiDAR systems, special requirements must be fulfilled. Their main operating range is below 50 m, which is equivalent to $0.3 \mu\text{s}$ according to (1). These small timing scales are more complicated to realize compared to long-range LiDAR systems with distances up to 2.5 km corresponding to $17 \mu\text{s}$. Furthermore, traffic scenarios include very short distances of about 1 m as well. Moreover, a fast testing of LiDAR systems in vehicles requires OTA testing without any modifications at the car or LiDAR system. Therefore, the trigger signal for the LTS must be achieved without electrical connection to the LiDAR system. In this work, we use an optical trigger of the LiDAR's laser signal causing a higher risk of undesired multipath reflections of this laser signal in turn, which must be considered as well for an automotive LTS. Although a flat screen with multiple optical triggers is mentioned in the patent [9], there is no discussion how to address the multipath reflection problem.

Our LTS is considered for all dToF LiDAR systems including scanning as well as flash systems and can be applied for different sensor types like avalanche photodiode (APD), single-photon avalanche diode (SPAD), silicon photomultiplier (SiPM) and photomultiplier tube (PMT). The following calculations refer to LiDAR with direct time-of-flight (dToF) but the basic principle of the LTS can be transferred to indirect time-of-flight (iToF) or frequency modulated continuous wave (FMCW) LiDAR as well to test the correct distance determination. Furthermore, FMCW LiDAR measures velocities directly, which could be considered additionally for the LiDAR target simulator. For dToF LiDAR system, the velocities are indirectly determined by distance measurements. Therefore, the validation of the distance measurements proves the velocity measurements as well.

A. Prerequisites

In the following investigations, the LiDAR range equation derived in [1] is applied to calculate photon event rates arriving at the LiDAR system (Fig. 3). In general, a LiDAR detector observes a diffuse target with Lambertian reflection. Within the equation, the optical power Ω_L of a laser with opening angle θ_L is distributed on a Lambertian target with defined distance d and reflectance ρ . The reflected light is received within the LiDAR field-of-view (FoV) θ_{FoV} by the LiDAR aperture with diameter D_{LiDAR} projecting the photons on a sensor with size a_{sensor} . In the LiDAR range equation, the photon event rate is given for one pixel with pixel FoV θ_{px} and size a_{px} . The required pixel FoV is calculated by

$$\Omega_{\text{px}} = \frac{A_{\text{px}}}{f^2}, \quad (2)$$

where A_{px} is the pixel area and f the focal length. The LiDAR system's laser solid angle is determined by

$$\Omega_L = \frac{A}{d^2}, \quad (3)$$

where A is a spherical area illuminated in distance d with either round or rectangular form [10]. Considering SPADs as most sensitive detector, the final expected photon event rate per pixel

TABLE I
PARAMETER VALUES OF EXAMPLE LIDAR SYSTEMS

Parameter	Symbol	Unit	Lange [11]	Beer [12]	Padmanabhan et al. [13]
Focal length	f	mm	2.6	12	15.4
Aperture diameter	D_{LiDAR}	mm	2.6	9.23	11
Pixel area	A_{px}	μm^2	12.5×14.5	40.56×52.4	240×240
Optical power	Φ_L	W	0.700	75	0.020
Laser opening angle(s)	θ_L	$(^\circ)^2$	50 (round)	40×1	20×20
Optics transmission	T	%	35	50	80
Fill factor	η_{FF}	%	100 ^a	5.32	50
PDP	η_{PDP}	%	65	1.89	10
Wavelength	λ	nm	630	905	780

Pixel area A_{px} is active optical area so that the fill factor is set to 100%.

becomes

$$r_{\text{target}} = \Phi_L \left(\frac{D_{\text{LiDAR}}}{2d} \right)^2 \frac{\min(\Omega_L, \Omega_{\text{px}})}{\Omega_L} \rho T \eta_{\text{FF}} \eta_{\text{PDP}} \frac{\lambda}{hc}, \quad (4)$$

where h is the Planck constant, c is the speed of light. The included minimum function considers scanning LiDAR systems where less target area is illuminated than one pixel observes with $\Omega_L < \Omega_{\text{px}}$. Otherwise, the illuminated target area is divided into the observed target areas by single pixels so that each pixel receives only the fraction $\frac{\Omega_{\text{px}}}{\Omega_L}$ of the total optical laser power.

The following considerations are supported by calculations based on the parameters of example LiDAR systems (Table I).

B. LTS Setup

The LTS consists of one optical trigger and multiple LTS sources representing different target points (Fig. 2). The laser signal of the LiDAR system is received by the optical trigger to determine the LiDAR measurement start. After that, the scenario simulation is performed by setting the required optical power and the ToF for the chosen scenario. These scenario settings can be generated in advance by a simulation or by real LiDAR measurement data. When the desired delay for an LTS source is achieved, the LTS source is triggered to emit the pulse answer with the determined optical power towards the LiDAR system. This simulated laser signal creates the desired scenario measured by the LiDAR system.

II. LTS SCREEN

We propose the LTS as a curved screen placed in front of the LiDAR system containing at least one optical trigger and multiple LTS sources (Fig. 4). The largest part of the screen consists of an antireflective surface to reduce undesired reflections of the LiDAR's laser signal back to the LiDAR detector. The LTS sources on the screen simulate the LiDAR environment. Each LTS source is approximately a point source with its own

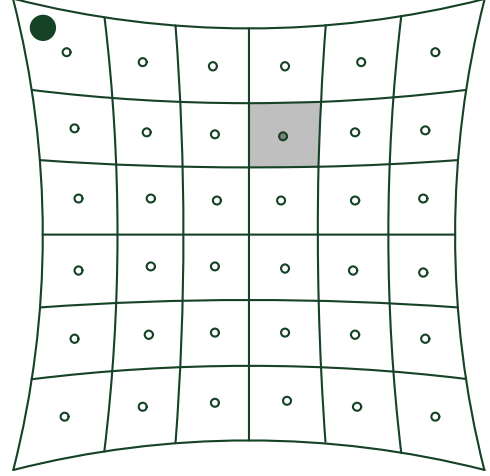


Fig. 4. Example of a curved LTS screen with 36 LTS sources and one optical trigger in the top left corner. One LTS source with area A_{src} is marked in dark gray with its LTS pixel area $A_{\text{LTS,px}}$ in light gray.

LTS pixel area $A_{\text{LTS,px}}$ of the screen representing the target area observed by one LiDAR pixel. The screen is positioned in front of a LiDAR detector with the LiDAR detector in the focal point of the arched screen. Thus, the distance from each LTS source to the LiDAR detector is equal. The LTS sources radiate perpendicular to the screen surface. Therefore, the center of each LTS source illumination lies in the center of the LiDAR detector. A vehicle with more than one LiDAR system can be tested by placing one LTS in front of each LiDAR detector. It is impossible to share one LTS for two LiDAR detectors at the same time because the angle and the distance from the LTS source to the LiDAR detectors would differ and hence require different irradiances (see Section III-A).

There are some restrictions on the screen that must be considered. Apart from a few exceptions, the LiDAR detector is placed in the image plane at the focal point of the lens collecting the light for the LiDAR detector. Within the depth of field (DoF), the LiDAR detector observes a proportional, sharp image of its environment. Therefore, the LTS screen must be positioned in the DoF to be sharply seen by the LiDAR detector as well. The largest DoF is reached if a LiDAR detector is set to image in almost infinite distance. This increases the beginning of the DoF and implies the largest blur in the near field. For the focus to infinity, the LiDAR detector is focused on the hyperfocal distance d_h . While the far point of the DoF lies in the infinite, the near point d_n is defined by half of the hyperfocal distance d_h with

$$d_n = \frac{d_h}{2} = \frac{f}{2} \left(1 + \frac{D_{\text{LiDAR}}}{z} \right), \quad (5)$$

where f is the focal length, D_{LiDAR} the receiver aperture diameter and z the circle of confusion (CoC) diameter [14]. For pixel detectors, the CoC corresponds to the pixel pitch. As the CoC must lie within one pixel, pixels are limited by their smallest dimension, which is the horizontal pixel pitch in most cases because the use of LiDAR systems for autonomous driving

TABLE II
MINIMUM SCREEN DISTANCE FOR EXAMPLE LiDAR SYSTEMS

Parameter	Symbol	Unit	Lange [11]	Beer [12]	Padmanabhan et al. [13]
Near point	d_n	m	0.08	1.37	0.26

often requires a larger horizontal FoV than vertical FoV. For different LiDAR systems, different near points occur (Table II). To guarantee that the screen stands within the DoF of most LiDAR detectors, the general screen distance is for example chosen to

$$s = 1.5 \text{ m}. \quad (6)$$

In general, the horizontal dimension of a LiDAR FoV is equal or larger than the vertical dimension for autonomous driving. Assuming a LiDAR FoV of $\theta_{\text{FoV,H}} \times \theta_{\text{FoV,V}} = 90^\circ \times 30^\circ$, the screen size is given by

$$A_{\text{LTS}} = s \cdot \theta_{\text{FoV,H}} \times s \cdot \theta_{\text{FoV,V}} = 2.4 \text{ m} \times 0.8 \text{ m}. \quad (7)$$

In general, the LTS screen can be larger but only LTS sources within the LiDAR detector's FoV contribute to the LiDAR measurement. Therefore, LTS sources at the screen margin outside the LiDAR FoV can be ignored or switched off. For a scanning LiDAR system, temporarily even more LTS sources can be switched off because only LTS sources that are currently illuminated and observed by the LiDAR system are required.

In the following, further screen properties are discussed.

A. Antireflective Screen

The own laser signal of the LiDAR detector must not be reflected by the screen and afterwards measured by the LiDAR detector. The easiest option would be to cover the laser source by an aperture including a hole for the optical trigger of the LTS. Especially for scanning LiDAR systems with moving or unknown laser origin, this solution is difficult to realize or even not practicable at all. Therefore, the laser signal must be absorbed by the LTS screen so that the remaining reflected light statistically produces a negligible signal at the LiDAR detector. As SPADs are one of the most sensitive LiDAR sensors, the following calculations are based on a known LiDAR system with SPADs so that the calculated parameters should resist for further unknown LiDAR systems. At first, the allowed event rates caused by the own laser signal must be determined. For example, a large distance measurement up to $d = 300 \text{ m}$ requires a measurement window of

$$t_w = \frac{2d}{c} = 2.0 \mu\text{s}. \quad (8)$$

Hence, the statistically self-induced event rate at one pixel of the LiDAR detector must be lower than

$$r_{\text{LTS}} = \frac{1}{t_w} = 500 \text{ kHz}. \quad (9)$$

Considering shorter measurement windows, this event rate can be even higher. The reflectance of the LiDAR's laser signal is caused by the screen itself, which is equivalent to the LTS

TABLE III
ANTIREFLECTIVE SCREEN PARAMETERS FOR EXAMPLE LiDAR SYSTEMS

Parameter	Symbol	Unit	Lange [11]	Beer [12]	Padmanabhan et al. [13]
Max. laser event rate by total LTS	r_{LTS}	kHz	500	500	500
Laser event rate by screen	r_{px}	kHz	0.001	0.53	0.02
Max. laser event rate by LTS sources	r_{src}	kHz	499.999	499.47	499.98
Max. LTS source reflection	ρ_{src}	%	100	100	100
Max. ND transmission	T_{ND}	%	0.05	0.05	0.05

pixel areas (light gray in Fig. 4) and the LTS sources on the screen (dark gray in Fig. 4) so that the event rate at the LiDAR detector is combined by

$$r_{\text{LTS}} = r_{\text{px}} + r_{\text{src}} \approx r_{\text{src}}, \quad (10)$$

where the screen reflectance is very low and hence negligible compared to the LTS source reflection as seen in the following (Table III). The illumination of the screen area itself is given by the ratio between the LTS source area A_{src} and the observed target area by a single pixel with

$$\Phi_{\text{px}} = \Phi_{\text{L}} \left(1 - \frac{A_{\text{src}}}{s^2 \Omega_{\text{px}}} \right). \quad (11)$$

The screen itself must have a surface with a low, diffuse reflection. Assuming a beam trap with reflectance of $\rho_{\text{screen}} = 10^{-6}$ [15], the LiDAR range equation leads to an event rate produced by the screen of

$$r_{\text{px}} = \Phi_{\text{px}} \left(\frac{D_{\text{LiDAR}}}{2s} \right)^2 \frac{\Omega_{\text{px}}}{\Omega_{\text{L}}} \rho_{\text{screen}} T \eta_{\text{FF}} \eta_{\text{PDP}} \frac{\lambda}{hc}. \quad (12)$$

One edge pixel additionally contains the optical trigger, which absorbs the incident light but can show a higher reflectance than the normal LTS pixel area. The reflection by a single LTS source area A_{src} with regards to the total illuminated target area A_{target} corresponds to the reduced optical power of

$$\Phi_{\text{src}} = \Phi_{\text{L}} \frac{A_{\text{src}}}{A_{\text{target}}} = \Phi_{\text{L}} \frac{A_{\text{src}}}{s^2 \Omega_{\text{L}}}. \quad (13)$$

The LTS source area has a higher reflectance than the screen and hence must be very small. This is realized by small holes in the screen, behind which the LTS sources are positioned (Fig. 5).

One LiDAR pixel must at least observe the whole LTS source area. Assuming hole diameters of $D_{\text{src}} = 100 \mu\text{m}$, the LTS source area becomes

$$A_{\text{src}} = \pi \left(\frac{D_{\text{src}}}{2} \right)^2 = 0.008 \text{ mm}^2. \quad (14)$$

This implies the condition that the minimum LiDAR laser opening angle or rather pixel FoV must be

$$\theta = 2 \arctan \left(\frac{D_{\text{src}}}{2s} \right) = 0.004^\circ. \quad (15)$$

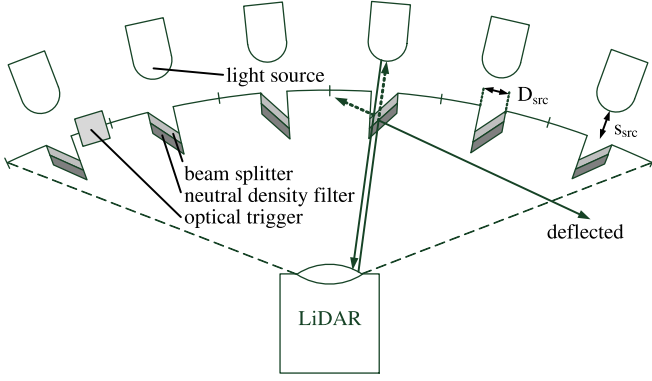


Fig. 5. Cross-section of LTS screen with antireflective functioning by beam splitters and neutral density filters.

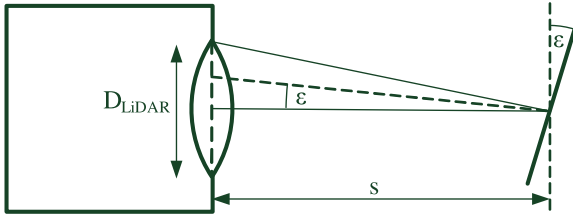


Fig. 6. Minimum mirror angle for deflection of LiDAR's laser beam.

In general, this condition is fulfilled so that the calculation of the optical power can be applied without further adaptations (see Section III-A). To avoid unnecessary reflections, the LTS sources are positioned behind the screen holes so that they illuminate not more area than required but minimum the total LiDAR aperture. Assuming a round LiDAR aperture with a maximum diameter of $D_{\text{LiDAR}} = 5 \text{ cm}$, the maximum distance between LTS sources and LTS screen is given by

$$s_{\text{src}} = \frac{s \cdot D_{\text{src}}}{D_{\text{LiDAR}} - D_{\text{src}}} = 3.0 \text{ mm}. \quad (16)$$

The reflectivity remains as adjustable parameter. Beam splitters are placed in front of the LTS sources (Fig. 5). The LiDAR's laser signal reflected by the beam splitter is deflected from the LiDAR detector while the transmitting proportion is reflected by the LTS source and after that divided again by the beam splitter. One proportion of the LTS source light can pass the beam splitter to illuminate the LiDAR detector while the other proportion is deflected. As the beam splitter affects both beam directions equally, the LTS source intensity must be increased to the desired value while the LiDAR laser signal remains reduced. All deflected light by LiDAR or LTS must vanish or be absorbed by the surrounding walls. For the deflection, the limiting LiDAR's laser beam is the central one (Fig. 6), which determines the minimum central mirror's angle to

$$\alpha = \frac{1}{2} \arctan \left(\frac{D_{\text{LiDAR}}}{2s} \right) = 0.48^\circ. \quad (17)$$

Each other mirror angle's absolute value can be chosen equal while the angle's orientation is radially symmetrical to the central laser beam. The mirror's diffuse proportion with reflectance ρ_{src} produces the remaining event rate by the reflection at the LTS source with

$$r_{\text{src}} = \Phi_{\text{src}} \left(\frac{D_{\text{LiDAR}}}{2s} \right)^2 \rho_{\text{src}} T_{\eta_{\text{FF}}} \eta_{\text{PDP}} \frac{\lambda}{hc}. \quad (18)$$

With (10), (12) and (18), the maximum reflectivity of the LTS sources can be defined by

$$\rho_{\text{src}} \approx \left(\frac{2s}{D_{\text{LiDAR}}} \right)^2 \frac{r_{\text{LTS}} hc}{\Phi_{\text{src}} T_{\eta_{\text{FF}}} \eta_{\text{PDP}} \lambda}. \quad (19)$$

If the beam splitter has a higher diffuse reflectivity, the irradiance must be further reduced by a neutral density (ND) filter in front of the beam splitter mirror. Most objects have no ideal Lambertian or specular reflection but a combination of both types just summed up [16]. Assuming a specular reflection proportion of $R_{\text{spec}} = 95\%$ of the incoming light, still $R_{\text{diff}} = 1 - R_{\text{spec}} = 5\%$ are diffusely reflected, which is equivalent to a totally diffuse reflection with reflectance

$$\rho_{\text{diff}} = \rho_{\text{mirror}} R_{\text{diff}}. \quad (20)$$

Assuming a beam splitter with reflectance $\rho_{\text{mirror}} = 1\%$, the neutral density filter must have a maximum transmission of

$$T_{\text{ND}} = \frac{\rho_{\text{diff}}}{\rho_{\text{src}}}. \quad (21)$$

As the neutral density filter applies in both optical ways, this optical light reduction must be considered for the optical power of the LTS sources as well (see Section III-A). For the chosen exemplary assumptions, the antireflective screen is realizable (Table III). The LTS screen reflection is negligible compared to the LTS sources reflection. For the chosen example parameters, the LTS source reflection always reaches the maximum of 100%. For 100% reflection, the corresponding ND requires a maximum transmission of $T_{\text{ND}} = 0.05\%$. Thus, the antireflective screen is easily realizable for all three example LiDAR systems.

B. Even LTS Screen

For easier construction, a screen only curved along one dimension or an even screen might be considered (see Section II-B). Assuming an LTS source at the corner of the example screen, the effects of a vertically even screen on an LTS source under angle α_{px} can be investigated (Fig. 7).

Then, the new screen distance of the LTS source becomes

$$s' = \frac{s}{\cos(\alpha_{\text{px}})}. \quad (22)$$

By the use of the trigonometric law of sine, the even dimension of the LTS pixel area is calculated (Fig. 8) resulting into

$$a'_{\text{LTS,px}} = \frac{2s' \sin \left(\frac{\theta_{\text{px}}}{2} \right)}{\cos \left(\alpha_{\text{px}} - \frac{\theta_{\text{px}}}{2} \right)}. \quad (23)$$

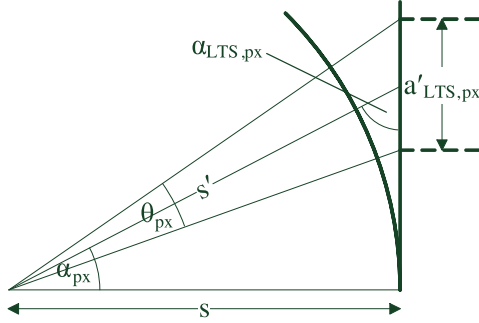


Fig. 7. Effects of vertically even screen on LTS source under angle α_{px} with regards to screen distance s' and LTS pixel area $a'_{LTS,px}$.

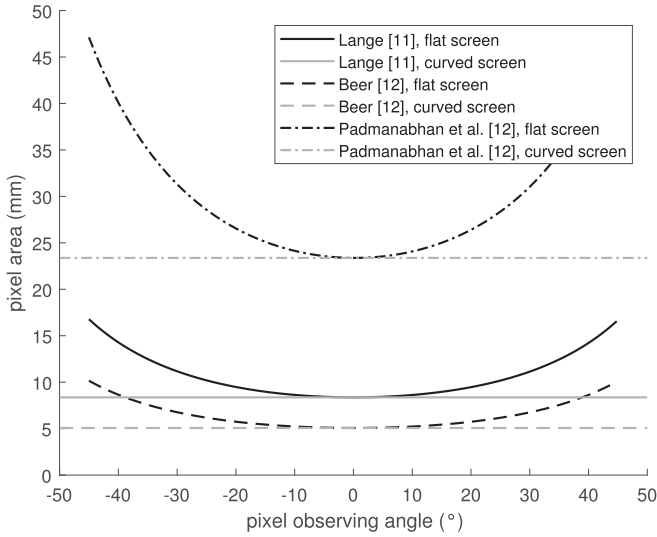


Fig. 8. Pixel size for flat or curved screen.

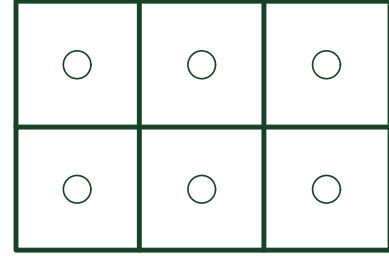
The LTS source orientation is no longer perpendicular to the LTS screen surface but is determined to be

$$\alpha_{LTS,px} = \arcsin\left(\frac{s}{s'}\right). \quad (24)$$

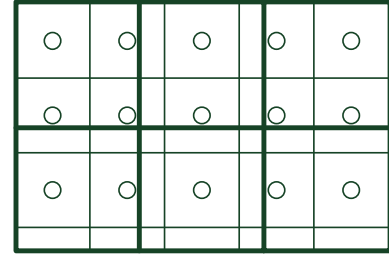
These new parameters can be calculated for each single LTS source to recalibrate optical power and ToF (see Section III-A and III-B). The edge LTS sources illuminate a larger flat area at the LiDAR system than the central LTS sources so that the illumination of the whole LiDAR aperture is guaranteed for each LTS source. However, the arrangement of the LTS sources is much easier on a curved screen.

C. LTS Sources Grid

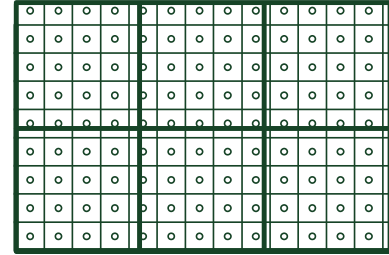
The largest part of the LTS screen is covered by a beam block or another antireflective material apart from the tiny LTS sources. As the LTS sources are discrete target points, one crucial difference to real targets is the inhomogeneity seen by the LiDAR detector due to the mismatch of discrete LiDAR pixels observing the discrete LTS sources with different grid size. One LTS source can either represent the target area seen by one pixel or describe an arbitrary point of the target. We discuss the three



(a) Matching LTS sources grid.



(b) Rematching LTS sources grid.



(c) Fine LTS sources grid, with LiDAR pixel observing most LTS sources (top center) and least LTS sources (bottom left).

Fig. 9. Possible LTS sources grids on LTS screen (thin grids) overlaid by grid of six LiDAR pixels observing the LTS screen (thick grid).

following possibilities to arrange the LTS sources grid on the LTS screen compared to the grid seen by the single pixels of the LiDAR system (Fig. 9).

1) *Matching LTS Sources Grid:* In the first case, the LTS sources must be distributed over the LTS screen so that each pixel FoV covers exactly one LTS source (Fig. 9(b)). For example, the smallest pixel observing angle of the example LiDAR systems (table I) is the horizontal one given by Beer [12] with

$$\theta_{px} = 2 \arctan\left(\frac{a_{px}}{2f}\right) = 0.2^\circ. \quad (25)$$

Such a pixel FoV results into an LTS pixel size of

$$a_{LTS,px} = s \cdot \theta_{px} = 5 \text{ mm}. \quad (26)$$

This matching of pixels and LTS sources allows an easy calculation of the required optical power of each LTS source while the disadvantage of this method is the customized rearrangement of the LTS pixel areas for the current LiDAR to be tested. The LTS pixel areas with surrounding antireflective surface are moved at the screen overlapping more or less until the LTS source areas match the pixel FoVs of each tested LiDAR detector. If not

declared otherwise, the matching case is chosen in the other considerations of this work.

2) *Rematching LTS Sources Grid*: Another possibility is keeping the LTS sources grid and the LiDAR pixel FoVs fixed. Then, some pixels observe more LTS sources than other pixels (Fig. 9(b)) so that rematching between the LTS sources grid and the LiDAR pixel grid is required. Therefore, the LiDAR pixel FoV must be known as well. With all known positions for each pixel, the number of matching LTS sources can be calculated. In contrast to the case of the matching LTS sources grid, the optical power provided for one pixel is not emitted by a single LTS source but distributed homogeneously over all concerned LTS sources. The matching grid is transferred to the rematching grid by redistributing the single LTS pixel area and optical power to all LTS sources within the pixel FoV.

3) *Fine LTS Sources Grid*: Alternatively, the LTS sources can be treated independently of the number of LiDAR pixels (Fig. 9(c)). The advantage is that the pixel FoV can be unknown and instead the optical power of the total LTS screen is calculated and then distributed on the single LTS sources. This mismatch becomes negligible if the LTS pixel area is very small compared to the observed target area by one LiDAR pixel. The most different pixel illuminations are given by LiDAR pixels observing all LTS sources of its observed LTS pixel areas (top center LiDAR pixel of Fig. 9(c)) and LiDAR pixels where every LTS source of the observed edge LTS pixels lies outside the LiDAR pixel FoV (bottom left LiDAR pixel of Fig. 9(c)). Assuming an LTS pixel area $A_{\text{LTS,px}} = a_{\text{LTS,px,H}} \times a_{\text{LTS,px,V}}$ and LiDAR pixel FoV $\Omega_{\text{px}} = \theta_{\text{px,H}} \times \theta_{\text{px,V}}$, the maximum uncertainty is given by

$$\sigma_{\text{mismatch}} = 1 - \frac{\left\lfloor \frac{s\theta_{\text{px,H}}}{a_{\text{LTS,px,H}}} \right\rfloor \left\lfloor \frac{s\theta_{\text{px,V}}}{a_{\text{LTS,px,V}}} \right\rfloor}{\left\lceil \frac{s\theta_{\text{px,H}}}{a_{\text{LTS,px,H}}} \right\rceil \left\lceil \frac{s\theta_{\text{px,V}}}{a_{\text{LTS,px,V}}} \right\rceil}. \quad (27)$$

With the chosen example pixel FoV of $\theta_{\text{px}} = 0.2^\circ$ and a desired maximum uncertainty of 5% between the LiDAR pixels, there must be between 39 and 40 times more LTS sources than pixels, which results to a maximum LTS pixel size of 0.1 mm. However, more LTS sources on the LTS screen increase the potential of unwanted back-reflections of the LiDAR's laser signal. Finally, such a large number of LTS sources might be impossible to realize considering very small LiDAR pixel FoVs.

III. SCENARIO SIMULATION

For the scenario simulation, the required optical power and time-of-flight must be provided as follows.

A. Optical Power

We derive a model to determine the optical power that must be set at the LTS source. The radiance provided by a single LTS source for a LiDAR pixel must be equal to the expected radiance reflected by a real target. With an exemplary LiDAR aperture of $D_{\text{LiDAR}} = 5 \text{ cm}$, the illumination angle of the flat area at the LiDAR detector is given by

$$\alpha_{\text{ill,flat}} = 2 \arctan \left(\frac{D_{\text{LiDAR}}}{2s} \right) \approx \frac{D_{\text{LiDAR}}}{s} = 2^\circ, \quad (28)$$

where the small angle approximation applies. In general, the irradiance of flat areas by point-symmetrical light sources is inhomogeneous with the largest irradiance at the center of the illuminated area but within such small angles the irradiance is approximately homogeneous. An LTS source with a spatially homogeneously distributed optical power Φ_{src} and opening angles $\theta_{\text{src,H}}$ and $\theta_{\text{src,V}}$ is assumed. The homogeneous irradiance of the LTS source at the LiDAR detector is given by

$$E_{\text{src}} = \frac{\Phi_{\text{src}}}{s^2 \Omega_{\text{src}}}, \quad (29)$$

with the solid angle Ω_{src} calculated equivalent to (3). To be more precise, the edge LTS sources illuminate a larger flat area than the central LTS sources, which can be additionally considered by $\cos^{-1}(\alpha_{\text{px}})$. It is assumed that a single pixel observes a homogeneous target area, which means a simulated target with almost perpendicular target orientation to the LiDAR detector and homogeneous reflectance over the whole target area. Special cases like different targets observed by a single pixel have to be discussed separately. They can be reduced to the homogeneous case by averaging all targets within a single pixel FoV. Besides the targets, direct light sources like other LiDAR's laser signals must be considered. In the following, the total optical power by a real target and the reflection possibilities are discussed.

1) *Optical Power by Real Target*: At first, the optical power per pixel transferred to the target Φ_{target} must be known. For a scanning LiDAR with a laser solid angle smaller than the pixel FoV with $\Omega_{\text{L}} \leq \Omega_{\text{px}}$, the optical power per pixel Φ_{target} is the optical power of the LiDAR laser Φ_{L} . In contrast to this, the optical power per pixel of a flash LiDAR is given by the proportion between the pixel FoV and the laser solid angle with

$$\Phi_{\text{target}} = \Phi_{\text{L}} \frac{\Omega_{\text{px}}}{\Omega_{\text{L}}}. \quad (30)$$

Due to the reflection, the optical power is reduced by reflectance ρ . The reflection type determines the reflected optical power received at the plane of the LiDAR detector. There are three possible reflection types. Most of the occurring reflections can be approximated by Lambertian reflections, which is an ideal diffuse reflection. In this case, each target area observed by a single pixel is approximated to be a point-like Lambertian reflection. Besides, there are specular reflections caused by mirrors or glossy surfaces. At last, there are retroreflectors at cars or as traffic signs that reflect the incoming light backwards to the emitting direction. Actually, most reflections are mixing types of diffuse and specular reflection, which can be assigned more or less to one of these both types.

2) *Lambertian Reflection*: Lambertian reflection means that the reflected power is distributed in the hemisphere with a maximum intensity along the direction parallel to the reflecting surface normal ($\theta = 0^\circ$), decreasing with $|\cos(\theta)|$ at larger angles θ . Therefore, the whole LiDAR aperture is illuminated, regardless of whether the target is illuminated by a flash or scanning LiDAR. If the target area is perpendicular to the LiDAR detector, the irradiance at the center of the LiDAR detector ($\theta = 0^\circ$) is given by the integral over a hemispherical shell

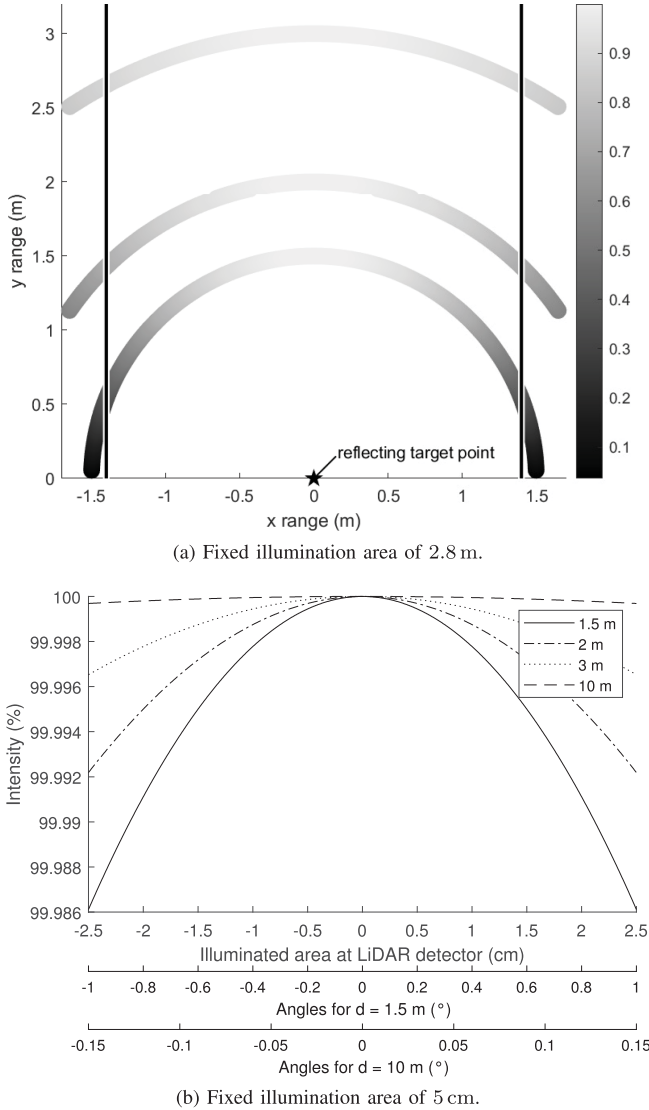


Fig. 10. Influence of target distance on Lambertian cosines distribution within fixed illumination area.

including the factor $\cos(\theta)$ resulting into

$$E_{\text{refl}} = \frac{\rho \Phi_{\text{target}}}{d^2 \pi}, \quad (31)$$

where the target distance d represents the radius of the hemispherical shell [1]. The irradiance E_{refl} delivered by a real target must be equal to the irradiance E_{src} produced by the LTS. Additionally, the beam splitter transmission T_{px} and ND filter transmission T_{ND} for the antireflective screen must be considered. Using (29) and (31), the final optical power of an LTS source results into

$$\Phi_{\text{src}} = \frac{s^2 \Omega_{\text{src}} E_{\text{refl}}}{T_{\text{px}} T_{\text{ND}}}. \quad (32)$$

In reality, the target distance determines the influence of the Lambertian cosine distribution within a fixed illuminated target area (Fig. 10). As the illumination angle is small, the irradiance at the center of the LiDAR detector is approximately the irradiance

at the whole LiDAR detector aperture. Therefore, this effect is negligible and it is sufficient if the distribution of the LTS source power is approximately homogeneous within the required illumination angle of (28). Hence, the Lambertian reflection is easily simulated.

3) *Retroreflection*: A retroreflector is constructed to reflect incoming optical power backwards to the incident direction so that the optical power is as high as possible for a nearly independent angle of incidence. The reflectivity R is determined differently for different types of retroreflectors and depends on the material reflectance ρ so that it lies around $R = 80\%$ to 90% [17]. Therefore, the received optical power at a pixel of the LiDAR detector and hence optical power of an LTS source is given by

$$\Phi_{\text{refl}} = \frac{R \Phi_{\text{target}}}{T_{\text{px}} T_{\text{ND}}}. \quad (33)$$

The irradiance at the LiDAR aperture is given by

$$E_{\text{refl}} = \frac{\Phi_{\text{refl}}}{A_{\text{LiDAR}}} = \frac{4 \Phi_{\text{refl}}}{\pi D_{\text{LiDAR}}^2}. \quad (34)$$

With the condition of equal irradiances, the required optical power of the LTS source equates to

$$\Phi_{\text{src}} = \frac{4 \Phi_{\text{refl}} s^2 \Omega_{\text{src}}}{\pi D_{\text{LiDAR}}^2}. \quad (35)$$

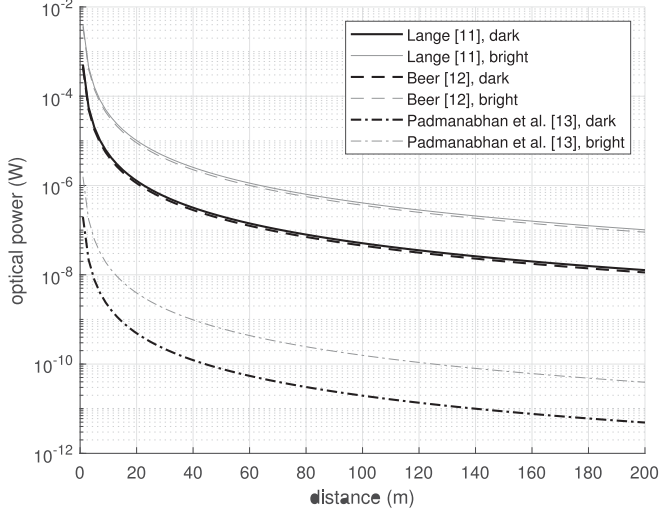
Depending on the retroreflector type, additional optical power losses might be considered.

4) *Specular Reflection*: If the specular surface is almost perpendicular to the LiDAR detector, the LiDAR laser light is reflected back to the LiDAR detector only reduced by reflectance ρ of the mirror material. Then, the optical power at the LiDAR detector becomes

$$\Phi_{\text{refl}} = \frac{\rho \Phi_{\text{target}}}{T_{\text{px}} T_{\text{ND}}}. \quad (36)$$

The concerning optical power of the LTS source is again determined by (34) and (35). As seen in (17), the maximum mirror angle for such a detection is very small. Because of the mirror's property to reflect light with the same angle of reflection as the angle of incidence, the laser signal is deflected from the LiDAR detector in most cases. Depending on mirror loss and next illuminated target after the mirror, there is either no signal at all measured by the LiDAR detector or instead of the mirror itself the next target is detected with measured distance as lighting path over the mirror to the final target and backwards. Each single reflection of this multipath reflection decreases the received optical power depending on each reflection type. Therefore, flat mirrors are often undetected and only concave mirrors with focussing properties like those of headlights can be problematic, which is not discussed here.

5) *Dynamic Range of Reflections*: The largest dynamic range of the reflected optical power is given by the Lambertian reflection with the strong dependency on the target distance whereby transmissions $T_{\text{px}} = 1$ and $T_{\text{ND}} = 1$ are assumed (Fig. 11 and Table IV). A low optical power is given by a far dark target, which is assumed by a target distance of 200 m and reflectance 10%

Fig. 11. Optical power of LTS sources Φ_{src} for example Lambertian targets.TABLE IV
OPTICAL POWER OF LTS SOURCES Φ_{src} (W) OF FIG. 11

Target type	distance (m)	reflectance (%)	Optical power (W)		
			Lange [11]	Beer [12]	Padmanabhan et al. [13]
Dark	200	10	$1.3\text{E} - 8$	$1.1\text{E} - 8$	$4.9\text{E} - 12$
Bright	1	80	$4.1\text{E} - 3$	$3.6\text{E} - 3$	$1.6\text{E} - 6$

here. In contrast, a high optical power is represented by a target at distance 1 m with reflectance 80%. For each LiDAR system, the relative dynamic range for these corner cases is determined to be

$$Q_{\text{target}} = \frac{\Phi_{\text{src,near,bright}}}{\Phi_{\text{src,far,dark}}} \approx 10^6. \quad (37)$$

With regards to the different example LiDAR systems, the optical power changes by the factor

$$Q_{\text{LiDAR}} = \frac{\Phi_{\text{src,Lange}}}{\Phi_{\text{src,Padmanabhan}}} \approx 10^3. \quad (38)$$

Therefore, delivering the dynamic range of both scenarios for all example LiDAR systems requires a total dynamic range of the LTS sources given by

$$Q_{\text{LTS}} = Q_{\text{target}} Q_{\text{LiDAR}} \approx 10^9. \quad (39)$$

Alternatively, a smaller dynamic range of the LTS given by the target dynamic range Q_{target} can be realized and the beginning of this dynamic range must be adjusted for each LiDAR detector. Another alternative would be the limiting of all testing scenarios to an even smaller dynamic range whose beginning is adjusted for each testing scenario if necessary.

6) *Direct Light Sources:* Direct light sources cause much higher signals at the LiDAR system than reflections. The optical power of a light source in distance d with optical power Φ_{light}

and solid angle Ω_{light} is given by

$$\Phi_{\text{light}} = \frac{\Phi_{\text{light}}}{d^2 \Omega_{\text{light}}}. \quad (40)$$

Again, the optical power of the LTS source is determined by (9) and (35). Due to the huge difference between the optical power by a target reflection and by a direct LiDAR's laser signal, it can be considered to use different light sources at each LTS pixel area for the simulation of reflecting targets and direct light sources separately. It must be considered that these additional light sources will increase the LTS screen reflectivity, which has been discussed above.

B. Time-of-Flight

The ToF of a virtual target is realized by the LTS via a delay between the emitted LiDAR's laser signal and the LTS source signal transferred back to the LiDAR detector. Simulating only one single laser shot, the minimum distance of the virtual target is the screen distance, which is actually traveled by the LiDAR's laser signal and the LTS source light. Additionally, electrical delays at the LTS are expected so that this minimum distance becomes even higher.

1) *Low Target Distances:* To simulate low target distances, the LTS can operate with one duty cycle delay. Therefore, the LTS estimates the arrival time of the next laser signal and emits its own LTS signal before receiving the LiDAR signal. This estimation is based on the calibration (see Section IV). Then, the simulation limit is not the screen distance but the beginning of the DoF. In operation under real conditions, the LiDAR detector would see a blurred image of its environment below the DoF. Contrary to this, the LTS in the LiDAR's DoF would still deliver a sharp image at low simulated target distances. If the LTS should simulate this blur effect, it can be calculated how much light is distributed beyond one pixel on its neighbor pixel by the CoC received of (5) with

$$z = \frac{f \cdot D}{2d_n - f}. \quad (41)$$

As the focal length f is not known in general and this method requires much effort, it will not be a practical solution. Anyway, the goal of the simulation of low distances must be considered. At these low distances, most LiDAR detectors are not constructed to distinguish targets in different pixels. Therefore, it is sufficient to test low target distances by the LTS if any signal is detected by the LiDAR detector than testing a realistically imaged scenario.

2) *Delay:* A delay element must be installed to wait for the next duty cycle for the simulation of low distances. In the automotive industry, a typical frame rate of $f = 25$ Hz might be desired, which corresponds to a time $t_{\text{frame}} = 40$ ms [18]. As seen in (8), the distance of $d = 300$ m corresponds to a ToF $t_w = 2$ μ s. Therefore, the coarse delay must be adjustable in steps of $t_w = 2$ μ s up to $t_{\text{frame}} = 40$ ms, which corresponds to a maximum number of steps of $n_{\text{coarse}} = \frac{t_{\text{frame}}}{t_w} = 20000$. The fine delay must be adjustable in steps of the timing resolution. Considering $t_{\text{bin}} = 312.5$ ps corresponding to a depth resolution of approximately 5 cm [12] and $t_w = 2$ μ s, this corresponds

to $n_{\text{fine}} = \frac{t_w}{t_{\text{bin}}} = 6400$ steps. These numbers of steps require counters with $\lceil \log_2(n_{\text{coarse}}) \rceil = 15$ bits and $\lceil \log_2(n_{\text{fine}}) \rceil = 13$ bits.

IV. CALIBRATION

The goal of the LTS is the testing of any LiDAR detector without previous knowledge. Therefore, the required LiDAR detector parameters are not taken from data sheets but must be measured as described in the following.

A. LiDAR Parameters for Optical Power of LTS Sources

Some parameters are required to determine the optical power of the LTS light sources (see Section III-A). These LiDAR detector parameters are laser opening angle, FoV, pixel FoV and laser pulse form meaning especially optical peak power and laser pulse width. With regards to the laser opening angle, the illuminated area at the screen is easily measured by an infrared sensitive camera, which delivers the horizontal and vertical laser opening angle. The laser pulse form can be measured by a photo diode connected to an oscilloscope. For a precise measurement, the photo diode must have a sampling rate higher than the inverse LiDAR timing resolution. Assuming a timing resolution of $t_{\text{bin}} = 312.5$ ps [12], the minimum photo diode sampling rate should be

$$f_{\text{PD}} = \frac{1}{t_{\text{bin}}} = 3.2 \text{ GHz}. \quad (42)$$

The peak of the laser pulse form is the required optical peak power and the full width half maximum (FWHM) is the laser pulse width. The pixel FoV is measured by moving a target through the pixel FoV. The target positions leaving a single pixel FoV and entering the next pixel FoV investigated in both dimensions, provides the horizontal and vertical pixel FoV dimension. In the same way, the total LiDAR FoV can be determined so that the number of pixels is known as well. The laser solid angle and the FoV are expected to approximately match for flash LiDAR systems.

B. LiDAR Parameters for Time-of-Flight

Providing the desired ToF by the LTS requires the knowledge about the beginning of the ToF. This beginning is detected by an optical trigger, e.g. in form of a photo diode, placed at the edge of the screen or rather the edge of the illuminated screen area by the LiDAR detector. As the optical trigger is an additional source of unwanted reflections of the LiDAR's laser signal, the optical trigger should not be placed at the center of the LTS screen, which is the most interesting testing part of the LiDAR system. According to the FoV of the current LiDAR detector, the LTS pixel area including the optical trigger can be repositioned. For a precise estimation of the ToF, the beginning of the ToF must be measured with the same timing resolution t_{bin} as the LiDAR detector uses. Obviously, it is practical to use the photo diode of the optical trigger for the measurement of the laser pulse form as well (see Section IV-A). In the following, special pulse patterns are discussed.

1) *Irregular Pulse Patterns*: Scanning LiDAR systems often have irregular pulse patterns on the different pixels due to their mirror movement. In this case, it is not necessary to measure every single pulse, which would require an optical trigger at each possible laser position on the screen leading to the worst case of one optical trigger per pixel. If the pulse pattern is well defined, only the beginning of the pulse pattern measured by a single optical trigger is needed. The respective ToF of each pixel can be calculated then. The same method holds for a LiDAR detector with different lasers that operate in an alternating mode with a defined pattern. For the measurement of the spatially distributed pulse pattern, the optical trigger can be moved from pixel to pixel during the calibration. The preferred option would be a calibration screen with as many optical triggers as there are pixels to avoid measurement uncertainties. With this, the number of required trigger inputs can be reduced.

2) *Unknown Pulse Patterns*: For a higher resistance against erroneous detections of undesired infrared light sources like laser signals of other LiDAR systems, some LiDAR systems vary their pulse pattern [19]. At the calibration, this pulse pattern must be recognized as well. Otherwise, the LTS is not able to predict the next pulse and can only provide target distances higher than the screen distance and the additional loss of time by electrical delays (see Section III-B). If the pulse pattern is spatially varied in an incomprehensible way, optical triggers for each different laser position must be placed on the LTS screen where the maximum number of optical triggers is the number of LiDAR pixels. Then LiDAR systems with arbitrary pulse pattern can be tested by the LTS.

C. Timing Resolution

Testing the desired timing resolution of a specific LiDAR system requires a sufficient LTS timing jitter according to the LiDAR timing resolution. The total LTS timing jitter depends on the jitter of the optical trigger or rather the photo diode σ_{trigger} , the electrical jitter between the incoming trigger signal and the LTS trigger signal provided by the controlling electronics σ_{ctrl} , the measurement uncertainty of the pulse pattern beginnings σ_{pattern} , where the later pulses can have a different laser jitter σ_{pulses} than the first one measured by the optical trigger and finally the jitter of the LTS source itself σ_{src} . The total LTS jitter is given by the root mean square (RMS) of all involved jitters with

$$\sigma_{\text{LTS}} = \sqrt{\sigma_{\text{trigger}}^2 + \sigma_{\text{ctrl}}^2 + \sigma_{\text{pattern}}^2 + \sigma_{\text{pulses}}^2 + \sigma_{\text{src}}^2}. \quad (43)$$

This LTS jitter must be smaller than the LiDAR timing resolution to guarantee precise testing.

V. CONCLUSION

The proposed LiDAR target simulator enhances an important testing strategy for LiDAR systems. Researchers already considered concepts for some sensor types and applications, but LiDAR systems in the automotive industry must fulfill different requirements. Here, we presented a concept and first general considerations as well as challenging parts to construct an automotive LiDAR target simulator. We propose a screen

curved in both dimensions as best option while the LTS source arrangement on a vertically even screen is more critical. We reduced unwanted reflections by the LTS screen using beam splitters and neutral density filters. As the fine LTS source grid is unpracticable and the rematching LTS source grid is complicated to calculate, we suggest the matching LTS source grid as best solution. The optical power of the LTS sources as well as their dynamic range and time-of-flight have been derived by simulated target properties and measured LiDAR parameters. In the future, the realization of an automotive LiDAR target simulator will be essential to guarantee efficient testing. The main advantages are the reproducibility of testing scenarios with defined target distance, target reflectance and environmental conditions like the weather. Additionally, the LiDAR target simulator is time-efficient, as it runs at any hour of the night and day and independent of daily weather conditions. At last, this testing method is cost-efficient compared to real driving tests because it requires no testing driver and avoids material consumption e.g. in scenarios with crash tests.

REFERENCES

- [1] P. Seitz and A. J. Theuvsen, *Single-Photon Imaging*. Berlin, Germany: Springer, 2011.
- [2] Safemove. Mar. 2017. [Online]. Available: www.elektronikforschung.de/projekte/safemove
- [3] T. Dallmann, J.-K. Mende, and S. Wald, "ATRIUM: A radar target simulator for complex traffic scenarios," in *Proc. IEEE MTT-S Int. Conf. Microw. Intell. Mobility*, 2018, pp. 1–4.
- [4] M. Engelhardt, F. Pfeiffer, and E. M. Biebl, "A high bandwidth radar target simulator for automotive radar sensors," in *Proc. 13th Eur. Radar Conf.*, 2016, pp. 245–248. [Online]. Available: ieeexplore.ieee.org/stamp/stamp.jsp?tp=&arnumber=7811693
- [5] J. L. Smith, "Concepts using optical MEMS array for lidar scene projection," in *Proc. Technol. Synthetic Environ., Hardware-in-the-Loop Testing VIII*, 2003, pp. 276–287.
- [6] Y. Gao *et al.*, "A programmable all-optical delay array for light detection and ranging scene generation," *IEEE Access*, vol. 7, pp. 93489–93500, 2019.
- [7] Lidar target simulator. [Online]. Available: www.adas-iit.com/sensor-simulation/sensor-fusion-test/lidar-target-simulator
- [8] R. H. Rasshofer, M. Spies, and H. Spies, "Testsystem für lidarsensoren," German Patent DE102 007 057 372, May 2009. [Online]. Available: <https://patents.google.com/patent/DE102007057372A1>
- [9] J. Werschnik, T. Preuti, and H. Häsel, "Testeinheit und verfahren zum prüfen einer LIDAR-Einheit für ein fahrzeug" German Patent DE102 019 106 129, May 2020. [Online]. Available: <https://www.freepatentsonline.com/DE102019106129.html>
- [10] C. J. Willers, *Electro-Optical System Analysis and Design: A Radiometry Perspective*. Bellingham, WA, USA: SPIE, 2013.
- [11] R. Lange, "3D time-of-flight distance measurement with custom solid-state image sensors in CMOS/CCD-technology," Ph.D. dissertation, Univ. Siegen, Siegen, Germany, 2000.
- [12] M. Beer, "SPAD-basierte sensoren für die lauffzeitbasierte distanzmessung bei hoher hintergrundlichtintensität," Ph.D. dissertation, Univ. Duisburg-Essen, Duisburg, Germany, 2018.
- [13] P. Padmanabhan, C. Zhang, and E. Charbon, "Modeling and analysis of a direct time-of-flight sensor architecture for lidar applications," *Sensors*, Basel, Switzerland, vol. 19, no. 24, pp. 5464–5490, Dec. 2019.
- [14] F. Träger, *Springer Handbook of Lasers and Optics*. Berlin, Germany: Springer, 2012.
- [15] Acktar blackened laser beam traps and blocks. [Online]. Available: edmundoptics.com/f/acktar-blackened-laser-beam-traps-and-blocks/39581
- [16] Wolff, "On the relative brightness of specular and diffuse reflection," in *Proc. IEEE Conf. Comput. Vis. Pattern Recognit.*, 1994, pp. 369–376.
- [17] A. Egidi, "Review of main optical retroreflectors," Istituto Nazionale di Ricerca Metrologica, Turin, Italy, Tech. Rep. RT 31/2018, 2018.
- [18] I. Maksymova, C. Steger, and N. Druml, "Review of lidar sensor data acquisition and compression for automotive applications," *Proc.*, vol. 2, no. 13, pp. 852–855, Dec. 2018.
- [19] L. Carrara and A. Fiergolski, "An optical interference suppression scheme for TCSPC flash lidar imagers," *Appl. Sci.*, vol. 9, no. 11, pp. 2206–2220, 2019.



Sara Grollius received the Bachelor of Science and Master of Science degrees in physics from the University of Wuppertal, Wuppertal, Germany. She is currently working toward the Ph.D. degree in the field of electrical engineering with the Fraunhofer Institute for Microelectronic Circuits and Systems, Duisburg, Germany. Her research is about the quality and reliability of light detection and ranging (LiDAR) systems, which determine target distances by the principle of direct time-of-flight.



Manuel Ligges received the Diploma and Doctorate degree in physics from the University of Duisburg-Essen, Duisburg, Germany. Until 2019, he was a Research Assistant and an Assistant Professor in the field of solid-state physics. He currently leads the Group of Optical Systems at Fraunhofer Institute for Microelectronic Circuits and Systems, Duisburg, Germany.



Jennifer Ruskowski studied physics with RWTH Aachen, Aachen, Germany. She received the Doctoral degree in sensor packaging methods with the University of Duisburg-Essen, Duisburg, Germany. She was with the Fraunhofer Institute for Microelectronic Circuits and Systems. From 2016 to 2020, she was responsible for the 3-D sensor research activities with the Fraunhofer Institute for Microelectronic Circuits and Systems. During this time, first LiDAR sensors were developed and presented. She is currently the Head of mobility. She promotes autonomous and emissions-free mobility by new sensor solutions.



Anton Grabmaier studied physics with the University of Stuttgart, Stuttgart, Germany, and specialized in semiconductor physics and measurement technology. His dissertation was focused on laser diodes. Since 2006, he has been a Professor with the University of Duisburg-Essen, Duisburg, Germany, and is currently the Director of the Fraunhofer Institute for Microelectronic Circuits and Systems, Duisburg, Germany.